Journal of Materials Chemistry C

Accepted Manuscript

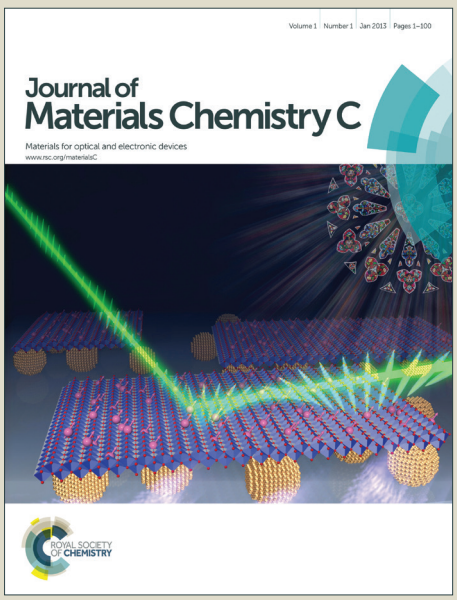

ROYAL SOCIETY OF CHEMISTRY

www.rsc.org/materialsC

Ag Decorated Topological Surface State Protected Hierarchical Bi_2Se_3 Nanoflakes for Enhanced Field Emission Property

Biswajit Das[a], Debabrata Sarkar[b], Supratim Maity[b] and Kalyan Kumar Chattopadhyay[a,b*]

[a]School of Material Science & Nanotechnology, Jadavpur University, Kolkata 700 032, India

[b]Thin Film &Nanoscience Laboratory, Department of Physics, JadavpurUniversity,Kolkata 700 032, India

*Corresponding author. Tel.: +91 9433389445; fax: +91 33 2414 600.

E-mail address: kalyan_chattopadhyay@yahoo.com (Kalyan Kumar Chattopadhyay).

Abstract

Here, we report an economical and low temperature synthesis route of Ag nanoparticle decorated hierarchical Bi_2Se_3 nanoflakes (NFs) over large surface area on the Si substrate in an open atmosphere. Detailed analysis of Field Emission (FE) property indicates that the hierarchical Bi_2Se_3 NF shows reasonable FE properties due to their high aspect ratio and well aligned uniform distribution. For improving the FE properties of as-synthesized Bi_2Se_3 NFs, silver (Ag) nanoparticles (NPs) have been attached on its surfaces. Ag NPs attached Bi_2Se_3 NFs exhibits superior FE property compared to the only Bi_2Se_3 NFs. The turn-on field is found to be reduced from 3.83 V/μm to 2.03 V/μm after attachment of the Ag NPs. Finite element analysis with ANSYS Maxwell simulation software also confirms that Ag decorated Bi_2Se_3 NFs are better field emitter than Bi_2Se_3 NFs. The enhanced FE properties of Ag attached Bi_2Se_3 heterostructure is attributed due to the electron injection from Ag nanoparticles to Bi_2Se_3 and also for the formation of extra emitting sites at the edge of the NFs. Finally, X-ray photo emission

spectroscopy (XPS) confirms that unlike most of the previous reports, surface states are appreciably stable and strongly protected from any surface reactivity and oxidation even if subjected to adverse atmosphere or high magnitude electric field.

Introduction:

Bismuth selenide is a well-known semiconducting material which was widely used for thermoelectric power generation and also for fabrication of infrared detectors because of its low energy band gap[1]. However recent interest in this material is due to the discovery of a different class of quantum material known as topological insulator (TI) having unique insulating bulk states which is encircled by conducting surface states[2,3]. Among all the chalcogen based 3D TIs materials, Bi_2Se_3 has single Dirac cone on its surface resulting in larger band gap around 0.3 eV[1], which enables numerous opportunities for room temperature applications. This material also possesses high electrical conductivity and less lattice thermal conductivity which make it to be a potential candidate for thermoelectric applications. Several groups[4,5] have worked on Bi_2Se_3 to evaluate the thermoelectric property of the same and reckoned the dimensionless figure of merit *ZT* much greater than one. A large number of scientific studies also reported diverse applications of this novel material in photosensitive devices[6], photo-electrochemical cells[7], and biological systems[8]. Sun et al.[9]have shown that Bi_2Se_3 exhibits long cycle of charging-discharging capacity indicating its application for hydrogen storage and high-energy batteries.

In last few decades, nanostructured materials have attracted much attention due to enhanced electron field emission performance originated from their high aspect ratio and proper aligned morphology[10]. Those field emitting materials are the potential candidates for display industry for making different types of field emission display units[11], back light for liquid crystal display panels and for many other electronic devices. From the structural point of view hierarchical

nanostructures of different semiconducting materials are better field emitter than normal nanostructures[12]. To increase the FE current density further at a low macroscopic field, different alternative techniques are employed, like coating with low work function semiconductor material[13] or by attaching appropriate metal nanoparticles[14] on the emitter surface. Literature survey indicated that reports on the field emission from Bi_2Se_3 nanostructures are extremely scanty. Yan et al.[15] studied the field emission property for Bi_2Se_3. However, they reported rapid surface oxidation upon atmosphere exposure and caused poor field emission performance. Oxidation occurring during cold electron emission process eventually decreases the FE performances of even well-known field emitters also[16]. A major challenge in FE devices is to protect the emitters from degradation upon application of high electric field. In this respect the recently discovered topologically surface states protected materials may be of significant use for such FE application. The aims of this paper is to investigate the FE properties of high quality Bi_2Se_3 hierarchical nanostructures, finding ways of improving its performance and also testing whether the Bi_2Se_3 samples can prevent surface modifications like oxidation[17] after FE operation.

So far, various nanostructures of different dimensions like nanoplatelets[18], nanoribbons[19], nanodiscs[20], nanorods[21]and hierarchical nanostructures[22] of Bi_2Se_3 have been synthesized by various routes like VLS[23], CVD[24], solvothermal[25], electro-deposition[26], SILAR[27] method and sono-electrochemical[28] deposition techniques. But most of the above synthesis techniques require difficult synthesis set-ups or very high deposition temperature introducing newer barrier in financial and industrial aspect. However, simple chemical bath deposition[22] technique is much appropriate in this regard because cost effective easy synthesis conditions like low synthesis

temperature (less than 100^{o}C) and normal atmospheric pressure are the only requirement for this method. Hence we have employed this CBD technique to synthesize Bi_2Se_3 hierarchical nanoflakes (NFs) in this work. Kong et al.[29] shown that topological insulating Bi_2Se_3 nanostructures and bulk materials are very much vulnerable under atmospheric oxidation even if in the normal ambient conditions. Tuning of nanostructural morphology may be an effective way out to overcome this drawback.

1. Experimental

All the chemical used in this study are of analytical grade and used as received without further purification. All aqueous solutions are prepared with deionized (DI) water.

2.1 Synthesis of Bi_2Se_3 Film

In a typical synthesis procedure, hierarchical Bi_2Se_3 NFs was grown on Si substrates using $Bi(NO_3)_3.5H_2O$ (99.99%) and Na_2SeSO_3 (99.99%) as sources of Bi^{3+} and Se^{2-} respectively. The chemical bath was prepared with 4 ml 0.1M $Bi(NO_3)_3.5H_2O$ and 80 ml 0.1M nitrilo-tri-acetic acid (NTA) to form the bismuth chelate. Under constant stirring 4 ml 0.5M ascorbic acid (AA) was added into the above mixture as reducing reagent. The pH of the solution was adjusted in between 8.50 - 9.00 by drop-wise addition of ammonia solution until a transparent solution was formed. 0.1M Na_2SeSO_3 solution was separately prepared by mixing 0.25 M Na_2SO_3 with 0.1 M Se powder at 85 ^{o}C under constant stirring condition for 10 h. 6 ml of that freshly prepared Na_2SeSO_3 solution was thereafter drop-wise added into the previous mixture solution. Commercially available p-type Si (100) wafers were chosen as substrates to deposit Bi_2Se_3 nanoflake thin films keeping in mind the universal application of Si as the most popular substrate material because of its usefulness in various devices. Prior to deposition, Si wafers were cleaned

with acid piranha and deionized water. Si substrates were immersed into the middle of the chemical bath and the deposition was carried out for 2.5 h maintaining the synthesis temperature at 75 ^{o}C. The optimum temperature, pH and other synthesis parameters were chosen according to the similar report by Sun et al.[22]. After the above mentioned period, the solution was allowed to cool naturally up to room temperature. The films were then taken out from the bath and rinsed several times with deionized water and ethanol, and dried naturally at room temperature.

2.2 Deposition of Ag Nanoparticles on Bi_2Se_3 Film

Ag NPs were synthesized on the hierarchical Bi_2Se_3 NFs films by reducing $AgNO_3$ using $NaBH_4$ and trisodium citrate (TSC-$Na_3C_6H_5O_7$) as stabilizing agent. In a typical procedure, as-fabricated Bi_2Se_3 hierarchical films were immersed in 30 ml of DI water for 30 min to remove excess free ions. 10ml of TSC (25 mM) was added to the solution and stirred continuously for 20 min at room temperature. To maintain the pH value of the solution above 7, NaOH solution was added drop-wise to the above solution. In another beaker 10 ml aqueous solution of $AgNO_3$ (0.1M) was taken and mixed with prepared solution. It was covered with aluminum foil and simultaneously this synthesizing procedure was performed under dark condition to minimize the exposure to light. The mixture was stirred continuously for another 20 min. Finally, freshly prepared 10 ml aqueous solution of $NaBH_4$ (25 mg/ml) was slowly added into the system under constant stirring for 2 h to confirm the complete reduction of Ag ions. The Ag NPs attached Bi_2Se_3 films were then removed from the reaction solution followed by washing with DI water several times. The as-prepared samples were then dried naturally and further characterizations were carried out with them. Fig. 1 schematically represents the typical steps for preparing hierarchical Bi_2Se_3 NFs and silver attached hierarchical Bi_2Se_3 NFs.

2.3 Characterization

The phase purity and crystallinity of the as-synthesized hierarchical Bi_2Se_3 NFs and Ag NPs attached hierarchical Bi_2Se_3 NF samples were investigated by a X-ray diffractometer (Bruker D8 Advanced) with Cu Kα radiation (λ=1.54056 Å, operating at 40 KV and 40 mA) in a 2θ range from 10^o - 60^o. The morphologies and microstructures of those samples were studied by field emission scanning electron microscopy (FESEM, Hitachi S-4800) at an accelerating voltage 5.0 kV. The chemical compositions as well as the spatial uniformity of the elemental distribution were analyzed by the energy dispersive X-ray spectroscopy (EDS, Thermo Scientific attached with Hitachi S-4800) operated at 15.0 kV. High-resolution transmission electron microscopic (HRTEM) studies as well as selected area electron diffraction (SAED) imaging were carried out by a JEOL 2010 TEM operating at an accelerating voltage of 200 kV to determine the exact dimension of the deposited Ag and to confirm the lattice spacing of both the host Bi_2Se_3 NFs and decorative Ag. Ionic states and composition of the hybrid system was analyzed via X-ray photoelectron spectroscopy (XPS) (HSA-3500, SPECS, German) using monochromatized Al Kα X-ray as the excitation source with energy of 1486.6 eV. Fourier transformed infrared spectra was obtained from Shimadzu FTIR-8400S. The field emission properties of the nanostructure films were examined inside a home made high vacuum chamber with a diode configuration setup. The nanostructure films were considered as a cathode and a stainless steel tip with diameter ~ 1 mm as an anode keeping the tip-sample separation ~ 180 μm by means of a micrometer screw.

2. Results and Discussion

The XRD patterns of the as-synthesized samples are shown in Fig. 2. The peaks in pattern (a) demonstrate the formation of the rhombohedra crystal phase of Bi_2Se_3, with lattice constants of $a=b=4.14$ Å, $c=28.63$ Å and space group *R3m* [JCPDS card no.33-0214]. The peaks near 38.18° and 44.36° were attributed to (111) and (200) planes of the face centered cubic (FCC) silver [JCPDS card no.04-0783].

The average crystallite size (L) of the hierarchical Bi_2Se_3 NFs, was determined to be 23.8 nm by using the following Debye-Scherrer formula[6, 30].

$$L = \frac{0.94\lambda}{\Gamma Cos\theta} \qquad \ldots(1)$$

Where λ is X-ray wavelength written above, Γ is the full width at half maximum (FWHM) in radian and θ is the Bragg's diffraction angle corresponding to the most intense (015) plane. Along with crystallite size, microstrain (ε) within the films and dislocation density (δ) of the samples were also calculated using the equations

$$\varepsilon = \frac{\Gamma cot\theta}{4} \qquad \ldots(2)$$

and

$$\delta = \frac{1}{L^2} \qquad \ldots(3)$$

Crystal size, microstrain and dislocation densities of synthesized hierarchical Bi_2Se_3 NFs are compared to other reports with respect to their synthesis time and temperature and the results are summarized in Table-1. From that tabulated results, we can conclude that film obtained in our work exhibit better crystallinity and less microstrain compared to others.

The morphologies of the as-synthesized films were studied by FESEM and the results are depicted in Fig. 3. The uniformity of those hierarchical NFs grown on the Si substrates is clearly observed in Fig. 3a, and the flakes length of the nanoflakes were measured to be of the order of 1.5 μm. The high magnification FESEM image (Fig. 3b) demonstrates that the nanoflakes have thickness in the range of 30-50 nm. It can also be observed that the nanoflakes are actually composed of thinner flakes having few nanometer widths. Silver NPs attached hierarchical Bi_2Se_3 NFs are shown in the Fig. 3c-d. The average size of these metal NPs varies from 10 to 30 nm in diameter as shown inFig. 3d.

The energy dispersive analysis of X-rays (EDX) pattern of the hierarchical Bi_2Se_3 NFs and Ag NPs attached hierarchical Bi_2Se_3 NFs are shown in Fig. 4a and 4b respectively. The EDX spectrum indicates that the Bi_2Se_3 sample is composed of Bi and Se with an atomic ratio of approximately 2:3 which is exactly expected for stoichiometric Bi_2Se_3. In Fig. 4b, a new peak at 2.97 keV can be observed which was attributed to $L\alpha^1$ line of metallic silver. Moreover, no additional peaks indicating the presence of impurities like oxygen or any other un-reacted precursor elements were detected in both the samples. These XRD pattern and the EDX spectrum both confirm the presence of elemental silver, which are attached to the Bi_2Se_3 NFs. To study the distribution of Ag NPs on the hierarchical Bi_2Se_3 NFs, the EDX mapping was performed which is shown in Fig. 4c-e. The results indicate that the Ag NPs are randomly distributed on Bi_2Se_3 NFs.

More detailed micro-structural information of the Bi_2Se_3 NFs was obtained by TEM. Fig. 5a and 5c clearly show a comparative feature of pristine Bi_2Se_3 NF and silver NP attached Bi_2Se_3 NF, respectively. The crystalline nature of those NF was studied by performing the selected area

electron diffraction (SAED) pattern, shown in the inset of Fig. 5a. The intense hexagonal symmetric spots demonstrate that the NF is highly crystalline in nature. A high resolution TEM (HRTEM) image at the edge of NFs demonstrates the layer like structure of Bi_2Se_3 (Fig. 5b). The corresponding pattern of those layers is shown in the inset of Fig. 5b. Inset of the Fig. 5c shows the HRTEM image of a single Bi_2Se_3-Ag hybrid structure. The lattice spacing ~ 0.305 nm and ~ 0.236 nm (Fig. 5d) represent the presence of (015) plane of Bi_2Se_3 and (111) plane of Ag which were also observed as the most intense peaks in their corresponding XRD pattern. The unaffected and straight lattice fringes and almost equal lattice spacing to that obtained from XRD analysis indicate that the Bi_2Se_3 flakes remained undistorted even after silver NP attachment and water contact.

The field emission current was measured and emission current density (J) is plotted as a function of applied electric field (E). The obtained results are shown in Fig. 6a. The FE behavior was quantitatively analyzed using the Fowler and Nordheim (F-N) [31] formula, which was solved by calculating the transmission probability of electrons through a triangular potential barrier due to the effective resultant of applied field and the image interaction. This F-N equation can be written as:

$$J = \frac{A E^2 \beta^2}{\varphi} exp\left(-\frac{B\varphi^{3/2}}{\beta E}\right) \quad \ldots(4)$$

and

$$ln\left(\frac{J}{E^2}\right) = \left(-\frac{B\varphi^{3/2}}{\beta}\right)\left(\frac{1}{E}\right) + ln\left(\frac{A\beta^2}{\varphi}\right) \quad \ldots.(5)$$

Where J is the current density; E is the applied field (V/μm); φ is the work function (eV); β is the field enhancement factor; A and B are constants with values 1.56 x 10^{-10} (AeV/V^2) and 6.38 x

10^3 (V/μm.eV$^{3/2}$), respectively. It has been proved by several studies that semiconductor nanostructures of GaS[32], ZnO[33], SiC[34]and CNT[35]show efficient FE behavior and their turn-on field strongly depend upon aspect ratio. The turn-on field and threshold field is defined as the field required to generate an emission current density ~ 10 μA cm^{-2} and ~100 μA cm^{-2} respectively. The turn-on fields and threshold fields were determined to be ~ 3.67 V μm^{-1} and ~ 7.44 V μm^{-1} respectively for hierarchical Bi_2Se_3 NFs and ~ 2.03 V μm^{-1} and ~ 3.83 V μm^{-1} respectively for Ag attached hierarchical Bi_2Se_3 NFs. It can be clearly seen that the turn-on field of hierarchical Bi_2Se_3 NFs is appreciably lower than the previous report concerning the FE properties of topological insulator Bi_2Se_3 NF film[15]. Yan et al.[15] explained the inferior FE properties of their samples by XPS analysis. They confirmed the presence of BiO_x and SeO_x peaks from XRS spectra and concluded that the oxidized surface states were responsible for high turn-on field and low FE current density.

The straight line nature of the F-N plot (in set of Fig. 6a) clearly indicates the cold emission behavior[31] of the samples. The typical work-function (φ) for both the materials are almost same (4.3 eV and 4.26 eV for Bi_2Se_3[15] and Ag[14] respectively) but the F-N plot of the Ag attached Bi_2Se_3 sample shows lower slope than pristine sample. Field-enhancement factor (β), defined as the ratio of the local field to the applied field [36] for both the samples were estimated from the slopes of FN plots. The average field-enhancement factors obtained to be ~ 5.79x10^3 and ~ 7.21x10^3 for hierarchical Bi_2Se_3 NFs and Ag attached hierarchical Bi_2Se_3 NFs respectively. Chen Li et al.[37]had shown that the β depends on some internal as well as external factors. These internal factors are mainly contributed by crystal structure, emitter geometry [36] and external factors like the screening contribution of the emitters, geometry of the underlying substrate[38]and emitters modified by decorating some metal NPs etc. are considered as external factors which

can affect field enhancement factor.Recently Ye et al.[39] and few other groups'[14]have shown that attachment of some novel metals like Pt, Au or Ag enhances the field emission property of most of the pure emitters. We also observed that after Ag NP attachment, β increased remarkably and emission current density considerably improved more than 10 times (~ 740 μAcm^{-2}) than the pure sample (~71μAcm^{-2}) measured at an applied field ~ 6.23 $V\mu m^{-1}$. The improvement of FE performance with Ag nanoparticle attachment is mainly due to two reasons. In addition to geometrical modification of Bi_2Se_3 NFs another aspect of Ag attachment might also be considered to play important role in enhancement of FE properties of the host Bi_2Se_3 NFs. It is well known that in case of metal/semiconductor (n-type) junction, Fermi level alignment due to junction formation occurs by carrier transfer between the two. The work function of Ag is less than the work function of Bi_2Se_3 as we have already mentioned, this favors[41]carrier transfer from Ag to Bi_2Se_3(figure S1) resulting in higher carrier density of the principal emitting Bi_2Se_3 NFs and higher emission current density was therefore observed in the hybrid system. Additionally Ag attachment to hierarchical Bi_2Se_3 NFs, Ag NPs creates sites around which the electric field intensity gets significantly enhanced (clear from simulation study discussed later). Ag NPs may also act as extra emitting sites. All these contribute to the increase in emission of current density and β. Table 2 comparatively represents various field emission parameters of Bi_2Se_3 samples in our work and other reports.However, we also analyzed the FE results taking into account the highest and lowest possible work functions of the hybrid system (i.e. considering the work functions of Bi_2Se_3 (4.3 eV) and Ag (4.26 eV) separately) to observe whether any change in values of β occurs at all. For this purpose, observed J-E curves were fitted with FN function. For this fitting we have chosen the work function as a parameter and calculated β from the best fitted curve. The fittings are shown in supporting information Figure. S2. The resulting enhancement

factors varied between 5847 (when fitting was done using Bi_2Se_3 work function) and 5758 (when fitting was done using Ag work function).

For the practical industrial application the field emission current stability is a major parameter for any emitting device. Fig. 6b demonstrates the emission current with respect to time over the 1.5 h duration for both the pure and Ag attached Bi_2Se_3 NF samples at a constant applied voltage of 1.6 kV. A little fluctuation in emission current during the testing period was observed for pristine Bi_2Se_3 NFs which disappeared resulting in stable emission for Ag NPs attached hierarchical Bi_2Se_3 NFs. This variation of current density may be accounted for factors like adsorption, desorption of residual gas molecules present in the ambience of the specimen, temperature of the emitting tips etc.

To investigate the effect of the shape of Bi_2Se_3 NF and origin of high current density after attachment of silver NP on it, we simulated the electrostatic field distribution based on the finite element method with ANSYS Maxwell simulation software package[42]. The 2D and 3D electric field distribution have been theoretically calculated for Bi_2Se_3 as well as Ag attached Bi_2Se_3 based cathodes with identical vertically aligned NFs. The modeling of those nanostructures was based on the typical morphology which we get from FESEM and TEM images. Electrode separation, type of the collector etc. were kept as actual experimental parameters. The obtained results are summarized in Fig. 7. A 2D semi cross-section of a single NF is shown in Fig. 7a, with height ~ 1.5 μm and width ~ 30 nm, which is placed on a Si substrate model and corresponding emitted field distribution is depicted. Similarly Fig. 7b shows Ag NP attached 2D semi cross-section of a single NF with emitted field distribution. The results clearly suggest that after attaching Ag NPs the average emission field have significantly increased almost 2 times

than that of the pure sample. To get closer results like actual experimental system, theoretical simulations were also carried out on 3 dimensional models with large number of identical inter connecting NFs. The top views of that 3D model without and with Ag NPs are shown in the Fig.7c and 7d, respectively. To analyze the field distributions for all the above models a rainbow color coordinate was employed with blue as the minimum and red symbolizing the maximum field. The simulated results clearly indicate that remarkable enhancement of emission field is expected for the attachment of Ag NPs upon Bi_2Se_3 NFs which is in good agreement with our experimental outcome.

We performed a series of perturbations, which are expected to affect the surface states of this Bi_2Se_3 NFs samples. The samples were (1) kept in open air for more than 6 months; (2) placed inside water for few hours while coating by Ag NPs on the surface and (3) high electric field was applied on the same during FE experiment; and finally the surface states of the samples were checked by X-ray photoelectron spectroscopy (XPS). XPS is the most reliable tool to identify the surface ionic states of elements. Fig. 8 shows the XPS spectra of the Ag attached Bi_2Se_3 NFs. The binding energy of the XPS spectra in Fig. 8 is calibrated by using the carbon C1s peak at 284.6 eV. In the survey spectrum (Fig. 8a), all of the peaks corresponding to elements Ag, Bi, Se, O, N and C were identified. The presence of trace amount of C, O and N in the above spectra is due to the atmospheric carbon, carbon dioxide or water vapor. But these gas molecules do not form any chemical bonds with Bi, Se or Ag which is confirmed by core level spectral scan over individual Bi 4f, Se 3d and Ag 3d states. The high-resolution spectrum of the Bi 4f shows (Fig. 8b) the spin-orbit splitting at 157.73 eV (Bi $4f_{7/2}$) and 163.03 eV (Bi $4f_{5/2}$) with a separation of 5.3 eV. This highly symmetric spectrum is fitted with the Gaussian plot which reveals that Bi is present only in single ionic state and no oxide formation occurred at all. This spin-orbit splitting

is shifted equally from the elemental Bi towards the higher binding energy[22, 43] (Table 3). Fig. 8c shows the Ag 3d spectrum is doubly split at 367.02 eV (Ag $3d_{5/2}$) and 373.05 eV (Ag $3d_{3/2}$) with binding energy difference ~ 6.03 eV. Interestingly, the binding energies of $Ag3d_{5/2}$ and $Ag3d_{3/2}$ peaks for the Ag NPs attached hierarchical Bi_2Se_3 NFs (concentration of Ag ~ 17 atom %) shifted to the lower binding energy. It is well known that monovalent Ag has much lower binding energy than that of zero valent Ag[44]. This shift therefore confirms that silver NPs are attached to the hierarchical Bi_2Se_3 NFs are in metallic silver[45] form. The presence of a broad peak at 52.97 eV in Fig. 8d corresponds to the Se 3d level[46]. The high-resolution Se 3d spectrum was de-convoluted into two peaks, and fitted by a single Gaussian curve with zero percent asymmetry with no trace of additional humps corresponding to any possible oxide states. The deconvoluted peaks at binding energies 52.8 eV and 53.7 eV are assigned for Se $3d_{5/2}$ and Se $3d_{3/2}$ respectively. The spin-orbit splitting spectral separation between these two states is almost 1.0 eV, which is in full agreement with the previous report (Table 3). The chemical shift is observed around the elemental Bi and Se positions are opposite to each other, indicating their opposite ionic states. Previous report demonstrated that Bi_2Se_3 surfaces were oxidized very quickly within few days[29]. However, as we have already mentioned that our samples were subjected to various external factors but remained unaltered as suggested by XPS results. We checked the Fourier transformed infrared spectra of the samples (FTIR), particularly in the water vapour absorption range (supporting Information, figure S3) and the same indicated no significant water adsorption. The topological surface states were successfully protected from the surface oxidation and this result is consistent with the report by Yashinaet al.[17]This may be considered as the main factor resulting in better FE properties of our samples unlike previous reports[15].

3. Conclusions

Well aligned uniform hierarchical Ag decorated Bi_2Se_3 NFs have been synthesized on Si substrate through a low cost and a low temperature chemical process. The FE property of hierarchical Bi_2Se_3 NFs has been investigated and low turn-on field ~ 3.83 V/μm is achieved. These results are significantly better than earlier reports of Bi_2Se_3 films. To confirm the presence of silver NPs XRD, EDX and XPS studies have been carried out. This enhancement of FE property was also investigated by simulation methods which also justify the experimental results. Surface states of the samples were strongly protected from oxidation and remained unchanged when kept in contact with air, water and subjected to high electric field, which was confirmed from XPS analysis. Single ionic states of Bi and Se were inferred symbolizing strong TI surface states. This synthesis route suggests that Bi_2Se_3 can preserve its topological surface states from severe external perturbations without any further passivation. The major advantage of this method is to develop low cost pure and metal assisted cold cathodes for emission based devices and the same is expected to show similar enhanced properties for several other applications too.

Acknowledgments

The authors like to acknowledge the financial support received from the University Grants Commission (UGC), the Govt. of India for 'University with potential for excellence (UPE-II)' scheme.

References

1. M. Z. Hasan and C. L. Kane, *Rev. Mod. Phys.,* 2010, **82**, 3045-3067.
2. Y. Yan, Z - M. Liao, Y - B. Zhou, H - C. Wu, Y - Q. Bie, J - J. Chen, J. Meng, X - S. Wu and D - P. Yu, *Sci. Rep.,*2013, **3**,1264.
3. H. Steinberg, J. B. Lalo¨ e, V. Fatemi, J. S. Moodera and P. Jarillo-Herrero, *Phys. Rev. B,* 2011, **84***,* 233101.
4. Z. Sun, S. Liufu, X. Chen and L. Chen, *ACS Appl. Mater. Interfaces,* 2011, **3**, 1390–1393.
5. A. Soni, Z. Yanyuan, Y. Ligen, M. M. K. Aik, M. S. Dresselhaus and Q. Xiong, *Nano Lett.,* 2012, **12**, 1203− 1209.
6. S. D. Kharade, N. B. Pawar, V. B. Hanwat, S. S. Mali, W. R. Bae, P. S. Patil, C. K. Hong, J. H. Kimd and P. N. Bhosale, *New J. Chem.,* 2013, **37**, 2821- 2828.
7. R. Jin, J. Liu, Y. Xu, G. Li, G. Chen and L. Yang, *J. Mater. Chem. A,* 2013, **1**, 10942-10950.
8. X. D. Zhang, J. Chen, Y. Min, G. B. Park, X. Shen, S. S. Song, Y. M. Sun, H. Wang, W. Long, J. Xie, K. Gao, L. Zhang, S. Fan, F. Fan and U. Jeong, *Adv. Funct. Mater.,*2014, **24**, 1718-1729.
9. Z. Sun, S. Liufu and X. C. L. Chen, *Chem.Commun.,* 2010, **46**, 3101–3103.
10. X. Fang, Y. Bando, U. K. Gautam, C. Ye and D. Golberg, *J. Mater. Chem.,* 2008, **18**, 509 – 522.
11. Y. Saito and S. Uemura, *Carbon,* 2000, **38**, 169 – 182.
12. F. Zhang, Q. Wu, X. Wang, N. Liu, J. Yang, Y. Hu, L. Yu, X. Wang, Z. Hu and J. Zhu, *J. Phys. Chem. C,* 2009, **113**, 4053-4058.

13. M. Deo, D. Shinde, A. Yengantiwar, J. Jog, B. Hannoyer, X. Sauvage, M. More and S. Ogale, *J. Mater. Chem.,* 2012*,* **22***,* 17055–17062.

14. S. S.Warule, N. S. Chaudhari, R. T. Khare, J. D. Ambekar, B. B. Kale and M. A. More, *Cryst. Eng. Comm.,*2013, **15**, 7475–7483.

15. Y. Yan, Z. M. Liao, F. Yu, H. C. Wu, G. Jing, Z. C. Yang, Q. Zhao and D. Yu, *Nanotechnology,* 2012, **23**, 305704 -305709.

16. A. Wadhawan, R. E. Stallcup, K. F. Stephens, J. M. Perez and I. A. Akwani, *Appl. Phys. Lett.,* 2001, **79**, 1867.

17. L. V. Yashina, J. S. Barriga, M. R. Scholz, A. A. Volykho, A. P. Sirotina, V. S. Neudachina, M. E. Tamm, A. Varykhalov, D. Marchenko, G. Springholz, G. Bauer, A. K. Gericke and O. Rader, *ACS Nano,* 2013, **7**, 5181– 5191.

18. D. Kong, W. Dang, J. J. Cha, H. Li, S. Meister, H. Peng, Z. Liu and Yi. Cui, *Nano Lett.,* 2010, **10**, 2245–2250.

19. H. Peng, K. Lai, D. Kong, S. Meister, Y. Chen, X. L. Qi, S. C. Zhang, Z. X. Shen and Y. Cui, *Nat. Mater.,* 2010, **9**, 225–229.

20. Y. Min, G. D. Moon, B. S. Kim, B. Lim, J. S. Kim, C. Y. Kang and J. U. Quick, *J. Am. Chem. Soc.,* 2012, **134**, 2872−2875.

21. S. Xu, W. Zhao, J. M. Hong, J. J. Zhu and H. Y. Chen,*Mater.Lett*., 2005,**59**, 319- 321.

22. Z. Sun, S. Liufua and L. Chen, *Dalton Trans,* 2010, **39**, 10883–10887.

23. Z. H. Wang, R. L. J. Qiu, C. H. Lee, Z. Zhang and X. P. A. Gao, *ACS Nano,* 2013*,* **7***,* 2126 – 2131.

24. W. Dang, H. L. Peng, H. Li, P. Wang and Z. Liu, *Nano Lett*., 2010, **10**, 2870-2876.

25. D. Kong, K. J. Koski, J. J. Cha, S. S. Hong and Y. Cui, *Nano Lett.,* 2013*,* **13***,* 632−636.

26. C. Han, J. Yang, C. Yan, Y. Li, F. Liu, L. Jiang, J. Ye and Y. Liu, *Cryst. Eng. Comm.,*2014, **16***,* 2823–2834.

27. C. D. Lokhande, B. R. Sankapal, S. D. Sartale, H. M. Pathan, M. Geirsing and M. Ganeshan, *Appl. Surf. Sci*., 2001, **182**, 413- 417.

28. X. F. Qiu, Y. B. Lou, A. C. S. Samia, A. Devadoss, J. D. Burgess, S. Dayal and C. Burda, *Angew. Chem. Int. Ed.,* 2005, **44**, 5855–5857.

29. D. Kong, J. J. Cha, K. Lai, H. Peng, J. G. Analytis, S. Meister, Y. Chen, H. Zhang, I. R. Fisher, Z. Shen and Y. Cui, *ACS Nano,* 2011, **5**, 4698 - 4703.

30. S. Subramanian and D. P. Padiyan, *Mater. Chem. Phys.,* 2008, **107**, 392–398.

31. D. Sarkar, C. K. Ghosh and K. K. Chattopadhyay, *Cryst. Eng. Comm.,*2012, **14**, 2683.

32. G. Sinha, S. K. Panda, A. Datta, P. G. Chavan, D. R. Shinde, M. A. More, D. S. Joag and A. Patra, *ACS Appl. Mater. Interfaces,* 2011,**3**, 2130–2135.

33. M. Deo, D. Shinde, A. Yengantiwar, J. Jog, B. Hannoyer, X. Sauvage and M. More, *J. Mater. Chem.,* 2012*,* **22***,* 17055–17062.

34. X. Zhang, Y. Chen, W. Liu, W. Xue, J. Li and Z. Xie, *J. Mater. Chem. C,* 2013,**1**, 6479.

35. N. Liu, G. Fang, W. Zeng, H. Zhou, H. Long and X. Zhao, *J. Mater. Chem.,* 2012*,* **22***,* 3478.

36. M. Zhang, T. Zhai, X. Wang, Y. Ma and J. Yao, *Cryst.Growth Des.,*2010, **10**, 1201–1206.

37. C. Li, Y. Di, W. Lei, Q. Yin, X. Zhang and Z. Zhao, *J. Phys. Chem. C,* 2008, **112,** 13447–13449.

38. S. Maiti, U. N. Maiti, A. Chowdhury and K. K. Chattopadhyay, *Cryst. Eng. Comm.,*2014, **16**, 1659-1668.

39. C. Ye, Y. Bando, X. Fang, G. Shen and D. Golberg, *J. Phys. Chem. C,* 2007, **111**, 12673-12676.

40. H. Huang, Y. Li, Q. Li, B. Li, Z. Song, W. Huang, C. Zhao, H. Zhang, S. Wen, D. Carroll and G. Fang, Nanoscale, 2014, **6**, 8306-8310.

41. B.G. Streetman and S. K. Banerjee, Solid State Electronic Devices, Pearson Prentice Hall, ISBN 978-81-317-0812-5, Sixth edition, 231.

42. S. Das, S. Saha, D. Sen, U. K. Ghorai, D. Banerjeeband and K. K. Chattopadhyay, *J. Mater. Chem. C,* 2014,2, 1321–1330.

43. V. B. Nascimento, V. E. de Carvalho, R. Paniago, E. A. Soares, L. O. Ladeira and H. D. Pfannes, *J. Electron. Spectrosc. Relat. Phenom.,*1999, **104**, 99–107.

44. S. A. Ansari, M. M. Khan, M. O. Ansari, J. Lee and M. H. Cho, *J. Phys. Chem. C,* 2013, **117***,* 27023-27030.

45. Q. Deng, X. Duan, D. H. L. Ng, H. Tang, Y. Yang, M. Kong, Z. Wu, W. Cai and G. Wang, *ACS Appl. Mater. Interfaces,* 2012, **4**, 6030−6037.

46. X. Yanga, X. Wangb and Z. Zhang, *J. Cryst. Growth,* 2005, **276**, 566–570.

Captions to the Figure

Fig. 1 Schematic of synthesis procedure of hierarchical Bi_2Se_3 NFs and silver attached hierarchical Bi_2Se_3 NFs prepared on the Si substrate.

Fig. 2 X-ray diffraction patterns: (a) the hierarchical Bi_2Se_3 NFs on Si substrate; (b) the Ag attached hierarchical Bi_2Se_3 NFs; (c) the Bi_2Se_3 JCPDS; (d) the Ag JCPDS and inset is the FWHM of the (105) peak of pure hierarchical Bi_2Se_3 NFs .

Fig. 3 FESEM images of: (a) the hierarchical Bi_2Se_3 NFs at low-magnification and the inset is the cross-section view of the NFs; (b) the hierarchical NFs at high-magnification; (c) the Ag attached hierarchical Bi_2Se_3 NFs; (d) at high-magnification different diameter ranges of Ag NPs are attached on hierarchical Bi_2Se_3 NFs.

Fig. 4 EDX spectra of (a) the hierarchical Bi_2Se_3 NFs; (b) the Ag attached hierarchical Bi_2Se_3 NFs (inset their corresponding images); and (c-e) the corresponding EDX elemental mapping which shows the distribution of Se, Bi and Ag, respectively.

Fig. 5TEM images of (a) Bi_2Se_3NF with SAED pattern in inset; (b) regular and parallel layers in flakes; (c) Ag attached Bi_2Se_3 NF with inset shows the high-magnification TEM image of white square region and (d) HRTEM image at the junction of Ag and Bi_2Se_3.

Fig. 6(a) Field emission current density versus applied field (*J*-*E*) curve of the pure hierarchical Bi_2Se_3 NFs (blue) and Ag attached hierarchical Bi_2Se_3 NFs (green) and Corresponding Fowler-Nordheim (*F*-*N*) plot shown in inset; (b) Field emission current stability (*I*-*t*) plot for the pure hierarchical Bi_2Se_3 NFs and Ag decorated hierarchical Bi_2Se_3 NFs.

Fig. 7 Simulation of electric field distribution of a sectional (a) Bi_2Se_3 NF; (b) Ag attached Bi_2Se_3 NF and (c-d) are top view of vertical 3D NF of Bi_2Se_3 and Ag NP attached Bi_2Se_3, respectively (inset corresponding side view).

Fig. 8 X-ray photoelectron spectra of the Ag attached hierarchical Bi_2Se_3 NFs: (a) Full spectrum of the sample; (b) Bi 4f spectrum; (c) Se 3d spectrum; (d) Ag 3d spectrum.

Table 1 XRD peak analysis in the reported literature

Sample	Plane	Crystalline size(L) in *nm*	Microstrain(ε)	Dislocation density(δ)x10^{-4} lines nm^{-2}	References
Hierarchical Bi_2Se_3NFs	(015)	23.8	0.006	17.71	This work
Bi_2Se_3	(015)	14.16	0.5713	49.90	6
Bi_2Se_3	(avg)	12.2	--	47.14	30

Table 2 Comparison of field emission characteristics of Bi_2Se_3 film with recent literature

Sample	Turn-on field at 10μA/cm^2	Threshold field at100μA/cm^2	Enhancement factor $\boldsymbol{\beta}$ ($\times \mathbf{10^3}$)	Reference
Bi_2Se_3nanoflake film	10.5V/μm	-	0.172	15
Bi_2Se_3nanosheets	2.3V/μm	-	6.860	40
Hierarchical Bi_2Se_3NF	3.83 V/μm	7.44 V/μm	5.79	This work
Ag NPs attached hierarchical Bi_2Se_3 NF	2.03 V/μm	3.67 V/μm	7.21	This work

Table 3 Literature comparison of peak position in the XPS spectra for Bi, Se and Ag

Transitions	Binding Energy (±0.1eV)for			Chemical Shift (±0.1eV)	References
	Elemental position	Bi_2Se_3 / Ag position(this work)	Bi_2Se_3 Reported		
Bi $4f_{7/2}$	156.6[*]	157.73	158.5[α]	1.13	43[*] 22[α]
Bi $4f_{5/2}$	161.9[*]	163.03	163.8[α]	1.13	43[*] 22[α]
Se $3d_{5/2}$	54.5[*]	52.8	53.2[ϰ]	-1.7	43[*] 46[ϰ]
Se $3d_{3/2}$	55.3[*]	53.8	53.95[ϰ]	-1.6	43[*] 46[ϰ]
Ag $3d_{5/2}$	368.2[ϛ]	367.02	---	-1.18	44[ϛ]
Ag $3d_{3/2}$	374.2[ϛ]	373.05	---	-1.15	44[ϛ]

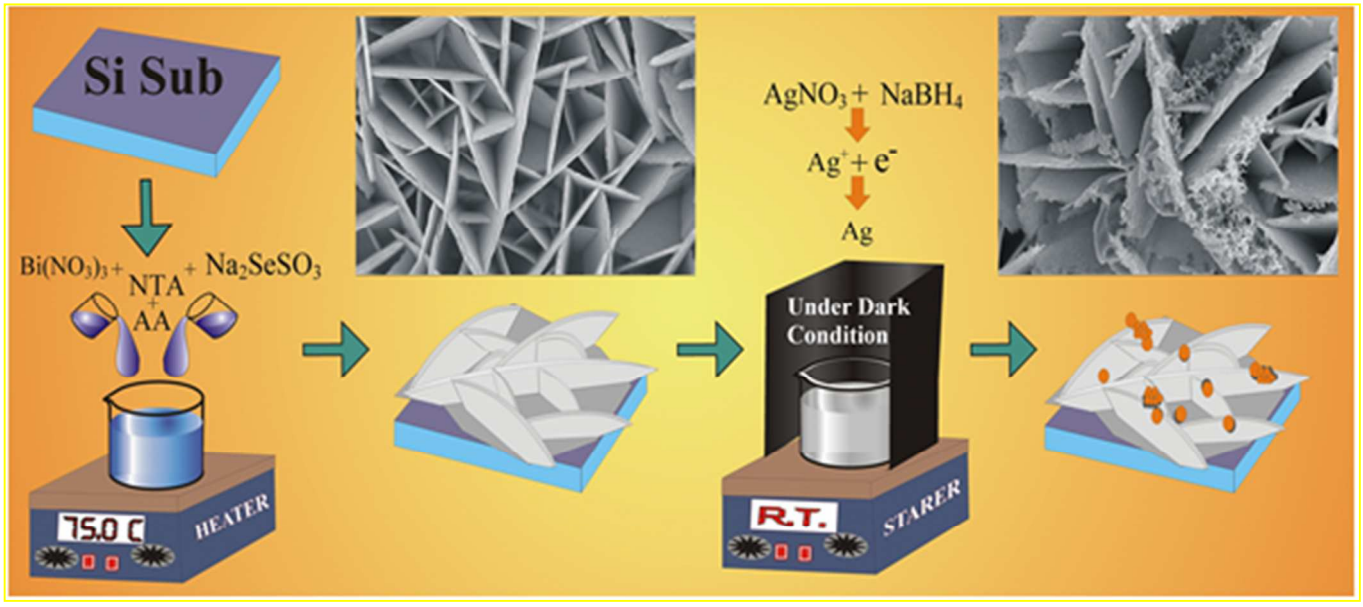

Fig. 1

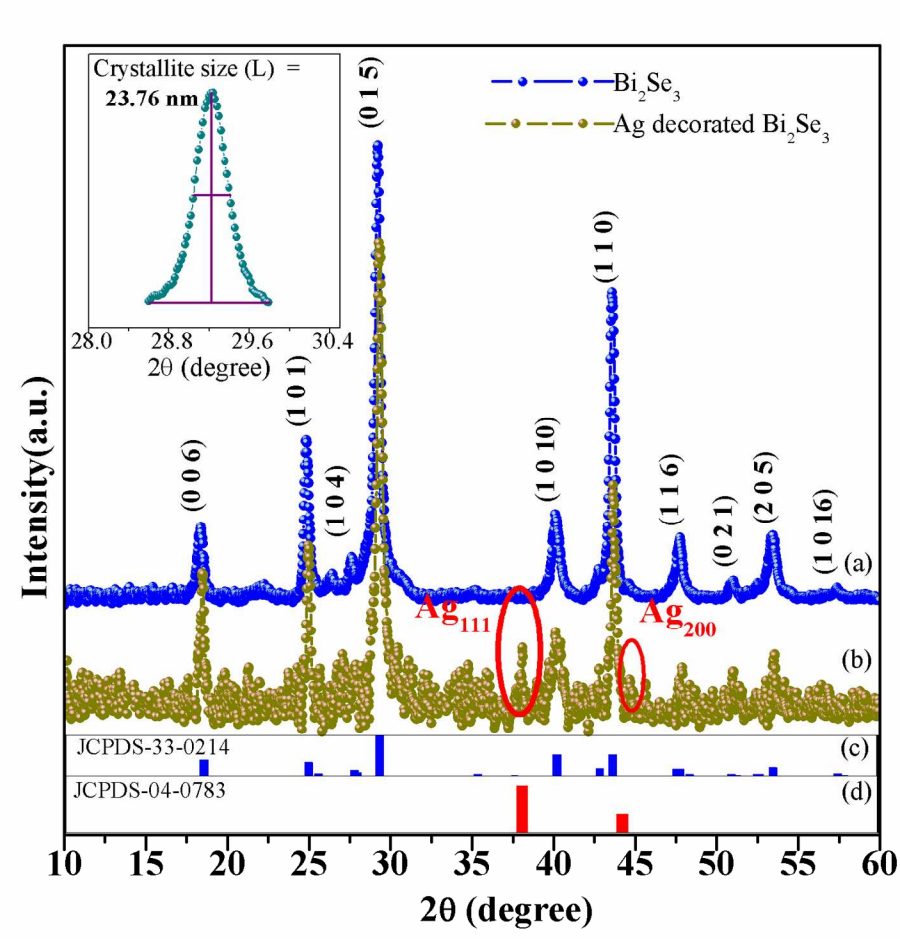

Fig. 2

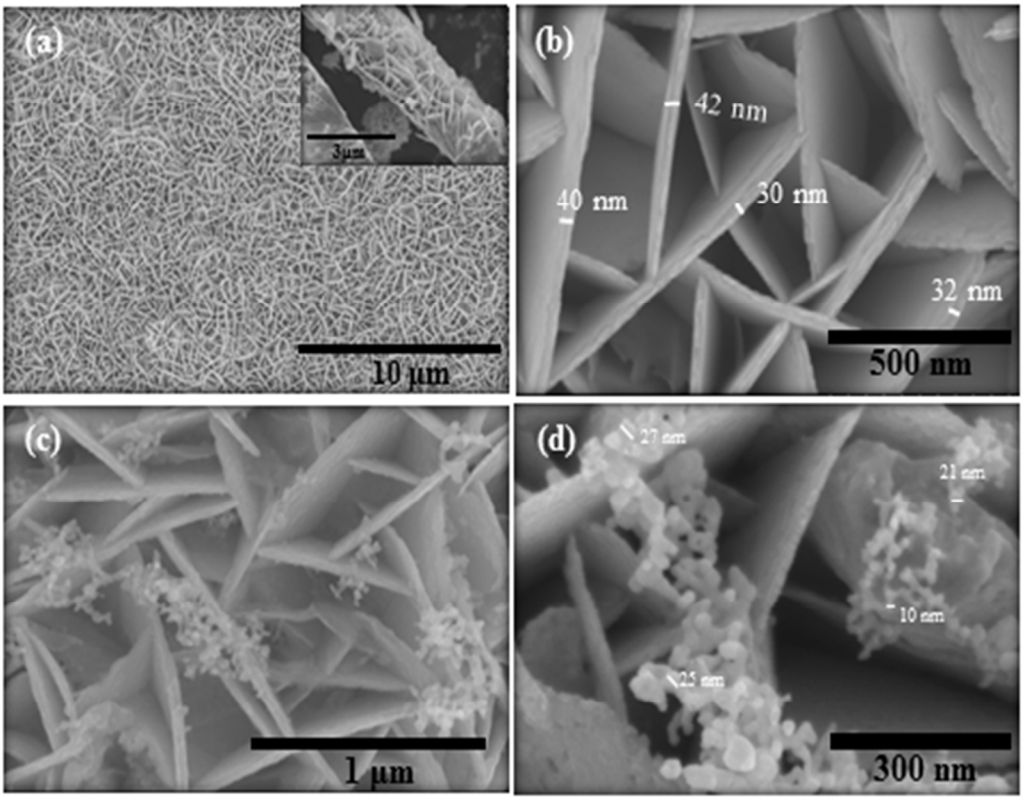

Fig. 3

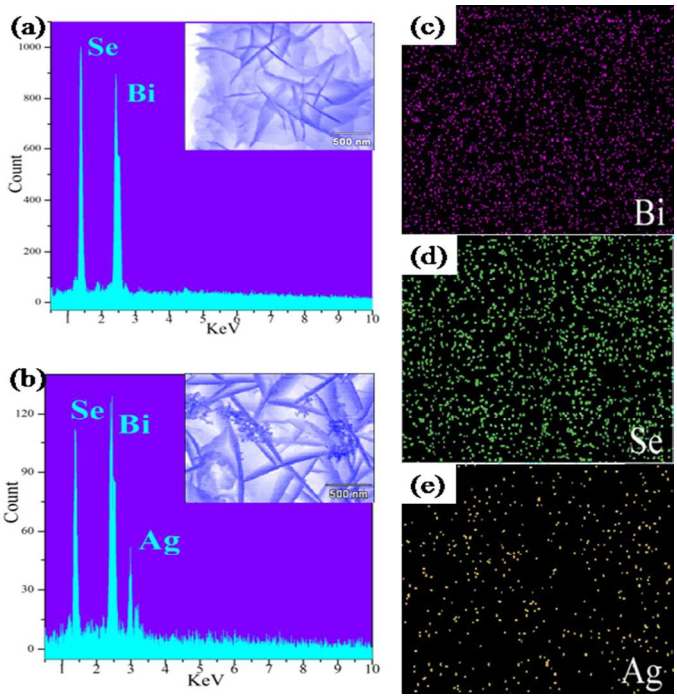

Fig. 4

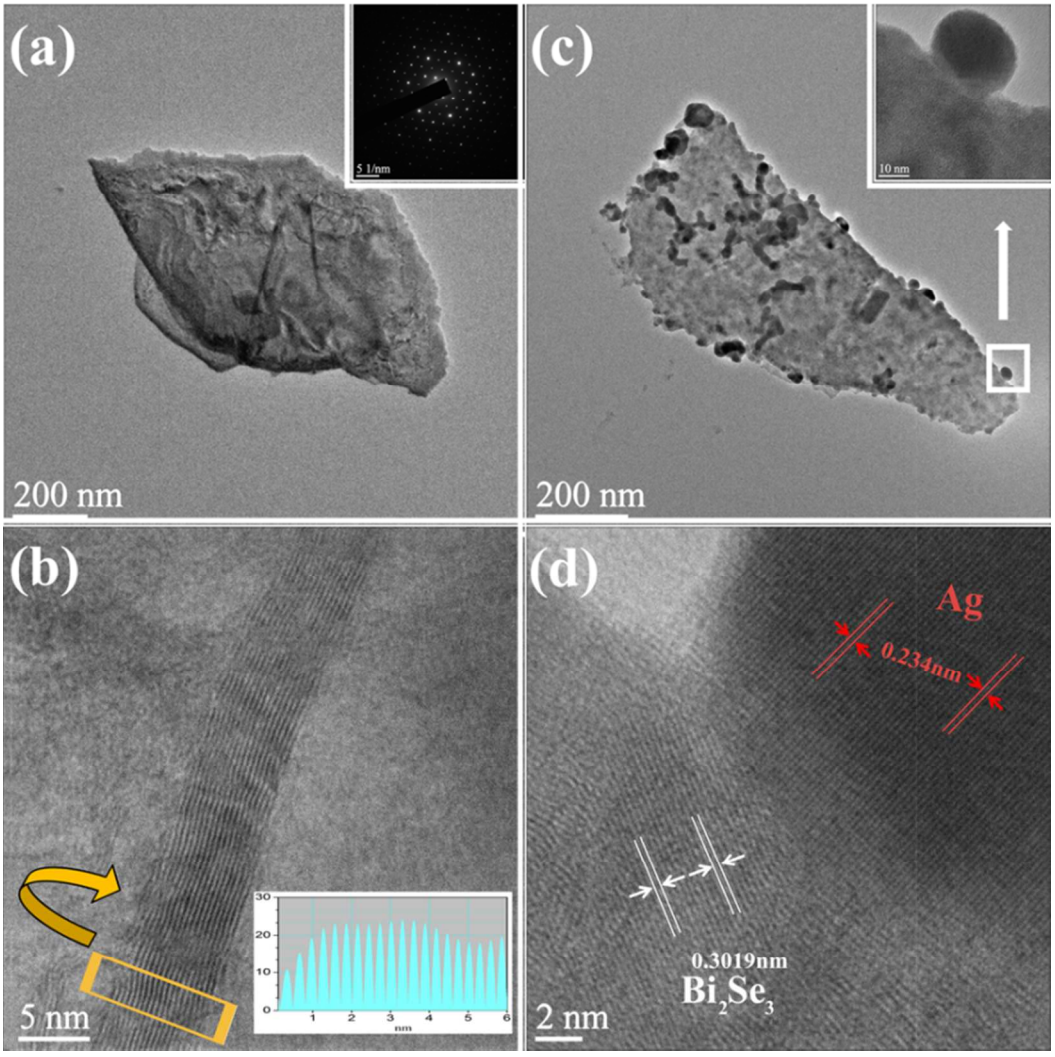

Fig. 5

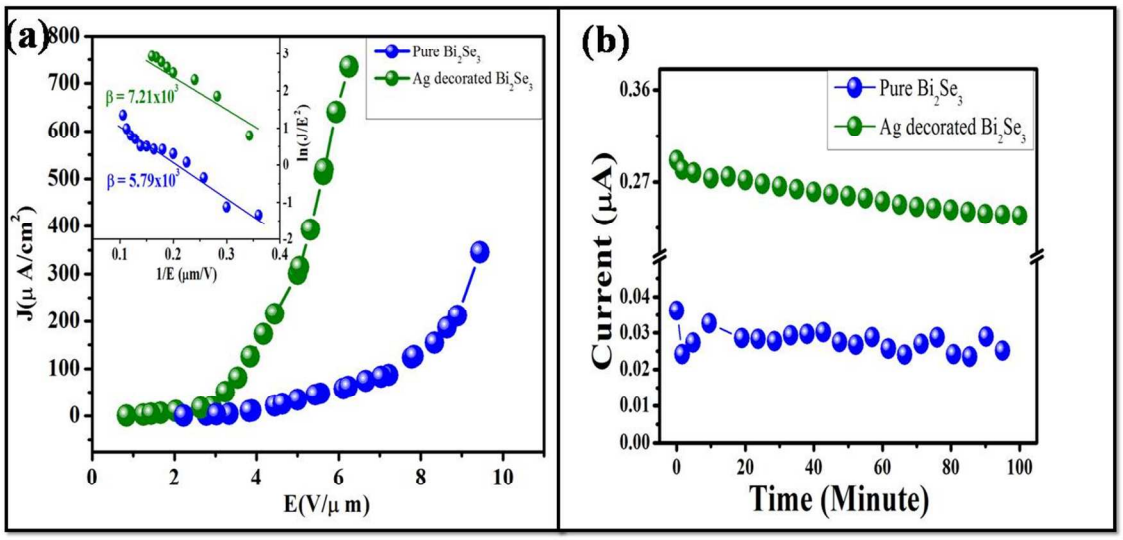

Fig. 6

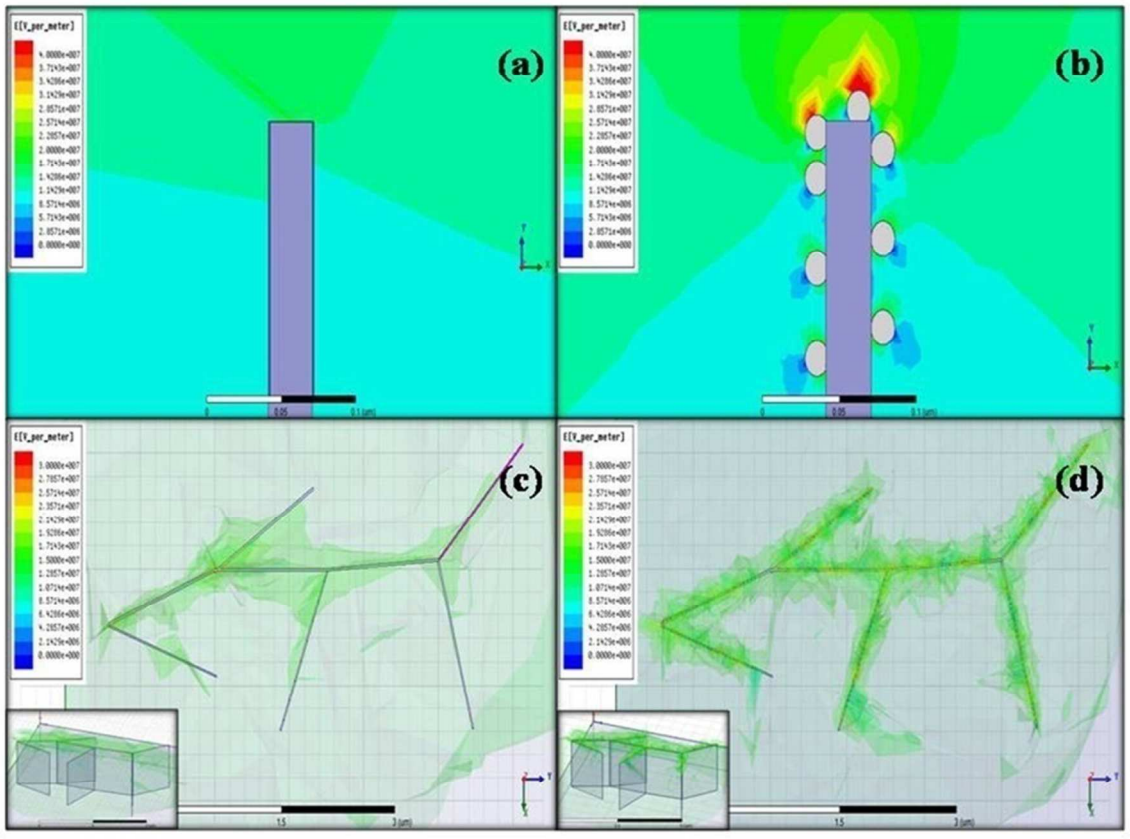

Fig. 7

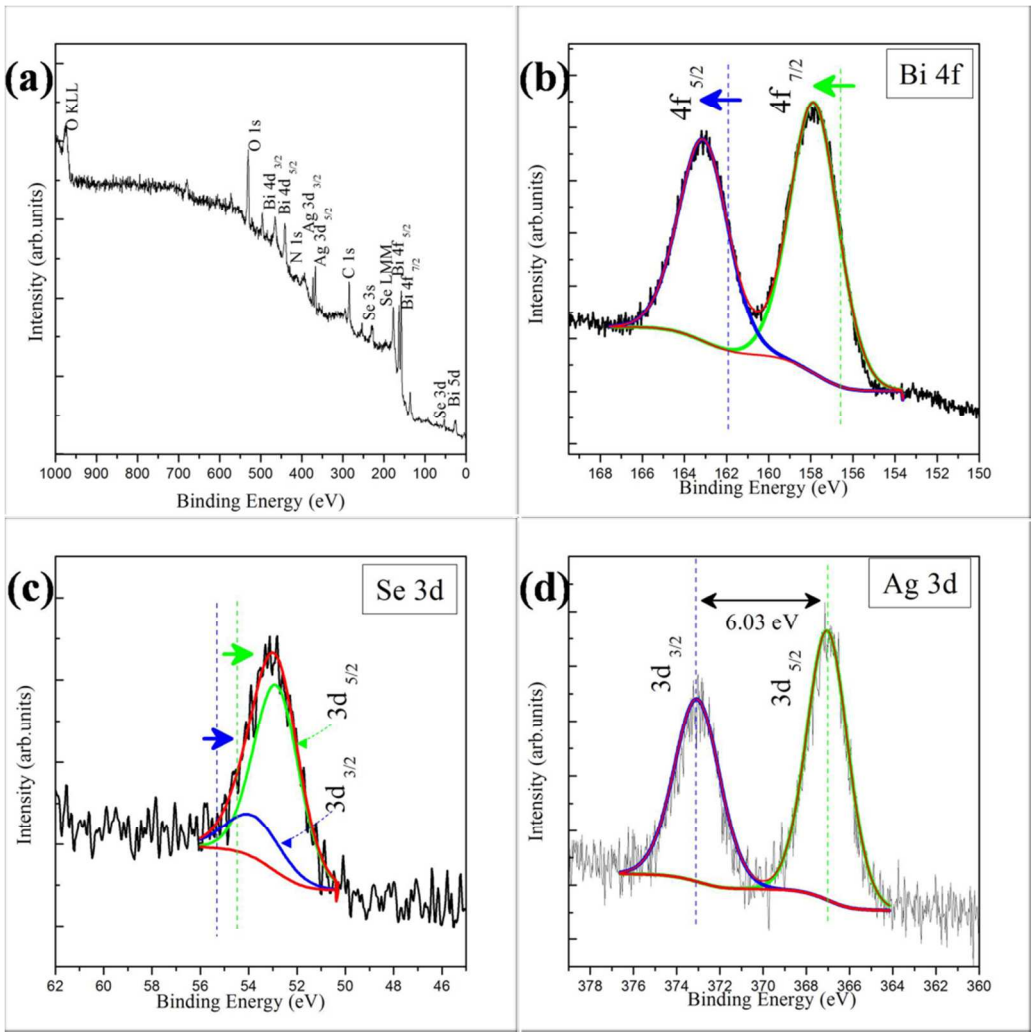

Fig. 8

Table of content